The influence of processing parameters on morphology and granulometry of a wet-milled sol-gel glass powder

Basam A.E. Ben-Arfa, Isabel M. Miranda Salvado, Robert C. Pullar, José M.F. Ferreira

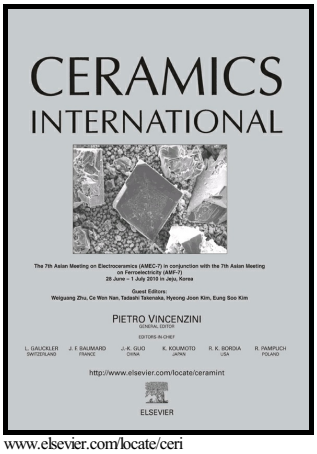

www.elsevier.com/locate/ceri

PII: S0272-8842(18)30951-9
DOI: https://doi.org/10.1016/j.ceramint.2018.04.080
Reference: CERI17997

To appear in: *Ceramics International*

Received date: 16 March 2018
Revised date: 9 April 2018
Accepted date: 10 April 2018

Cite this article as: Basam A.E. Ben-Arfa, Isabel M. Miranda Salvado, Robert C. Pullar and José M.F. Ferreira, The influence of processing parameters on morphology and granulometry of a wet-milled sol-gel glass powder, *Ceramics International,* https://doi.org/10.1016/j.ceramint.2018.04.080

The influence of processing parameters on morphology and granulometry of a wet-milled sol-gel glass powder

Basam A. E. Ben-Arfa, Isabel M. Miranda Salvado*, Robert C. Pullar*, and José M. F. Ferreira

Department of Materials and Ceramic Engineering / CICECO – Aveiro Institute of Materials, University of Aveiro, 3810-193 Aveiro, Portugal

Abstract

A quaternary bioactive sol-gel glass of high silica content was heat treated at different temperatures, and then wet ball milled under different balls to powder ratios. A total of sixteen experiments were performed to study in detail the effects of both experimental variables on the structure, morphology, particle size distributions and nitrogen adsorption isotherms. The balls–to–powder ratio exerts a tremendous influence on the final particle size distribution of the powders, while its effects on the pore volume and morphology are minimal. These structural features are mostly governed by the changes in calcination temperature. Therefore, understanding the specific roles of each experimental parameter is of paramount importance towards achieving optimum powders with the desired properties. This work sheds light on the importance of using a suitable combination of these two parameters for tuning the morphology and the granulometry of the sol-gel derived bioactive glass powders.

Keywords: Powder; Heat treatment temperature; Wet ball milling; Particle size distribution; Nitrogen adsorption isotherms.

1. Introduction

Powdered raw materials are widely used to produce ceramics in many industrial sectors (1). The ceramic parts can be shaped either by dry or wet powder processing routes. The dry processing route includes pressing the powder to form a green body, and often requires the addition of processing additives such as binders to assist in the consolidation process, and to confer enough strength to the green bodies to enable safe handling and densification behaviour along the subsequent processing steps (2). The wet routes involve mixing the powders with a compatible liquid in the required proportions, and adding suitable amounts of processing additives with different roles, which might include dispersants, binders, plasticisers, thickening agents, etc.. The aim is to obtain homogeneous mixtures, and to confer on them suitable rheological properties for the selected shaping technique. The traditional wet consolidation techniques might start from: (i) relatively concentrated pastes of clayey based materials or of advanced ceramics plasticised with suitable processing additives, and be accomplished by plastic forming (extrusion, roll forming, or jiggering) (3); (ii) fluid suspensions that consolidate upon partially removing the liquid by slip casting (4) or pressure casting (5), or by evaporation such as in tape casting (6).

However, it was shown that liquid removal driven by the capillary suction exerted by plaster moulds (slip casting), eventually assisted by an external applied pressure (pressure casting), is prone to lead to particle segregation by a process known as the clogging effect (7). This segregation mechanism is particularly favoured when fine particles are free enough to move quickly along with the liquid, under the effects of driving forces, leaving behind the coarser and heavier ones. In other words, all the factors that contribute to lowering the viscosity of the medium (high degree of

dispersion, decrease in solids loading) enhance this phenomenon. On the other hand, the deposition kinetics also determine the extent of particle segregation. It was shown that the driving force exerted by plaster moulds (about 0.15 MPa) maximised the clogging effect. Lower driving forces favoured segregation by sedimentation, while higher ones did not allow the particles to order in the highest possible packing arrangements (7). Aiming at overcoming the drawbacks of wet consolidation techniques involving liquid removal, and further exploring the potential advantages of colloidal processing, a number of direct consolidation techniques have been developed. Homogeneous suspensions are cast in non-porous moulds, and transformed into rigid bodies without liquid removal, thus preserving the homogeneity achieved in the starting suspensions. The consolidation can be achieved through different setting mechanisms, including, Starch Consolidation (8), Gel Casting (9), Direct Consolidation Casting (10), Hydrolysis-Assisted Solidification (11), Temperature Induced Gelation (12), Epoxy Gel Casting (13), etc.. Direct consolidation techniques enable the reduction of the number and the size of structural defects, thus enhancing the reliability of the advanced ceramics, and expanding the applications of colloidal processing. To achieve high green density and the desirable final properties (14), particle size (PS), particle size distribution (PSD) and particle morphology of the powders, and all the relevant processing parameters need to be optimised. This also applies to the modern additive manufacturing techniques when starting from powders, as in 3-D printing (15), or from extrudable pastes for robocasting (16). All of these motives justify a renewed emphasis on controlling the properties of the powders involved in the processing of ceramic and glass materials.

The reduction in particle size occurring during milling results from the accumulated stresses inside the particles due to the applied mechanical energy, which induces cracks that propagate through them, leading to particle breakage (17).

Particle breakage, comminution, pulverisation and milling are all interchangeable terms, commonly used with apparently identical meanings. The powder milling process may be conducted under dry conditions (dry milling) or in wet environments (wet milling). The later one is more efficient, commonly being recommended when high surface energy induces agglomeration between particles (18).

Many important parameters should be taken into consideration while performing wet ball milling. For example, the liquid-to-powder ratio (LPR), i.e., the solids loading, the type of milling machine, and the speed at it works, need to be selected according to the rheological behaviour of the suspension (19). Increasing heat treatment temperatures gradually lead to the formation of hard agglomerates that are difficult to destroy on milling, which strongly affect the microstructure and the properties of the final products. A few examples include power transmission (20), optical properties (21), photocatalytic activity (22,23), drug loading and release (24), phase transformations (25), and sintering ability (26). The effects of milling ball–to–powder ratio (BPR) on phase formation, and the resulting crystallite size, have been particularly investigated in works related to mechanochemical synthesis (27–29). However, most of these studies aimed at disclosing some interdependencies between the experimental variables and the measured properties for certain particular applications.

To the best of the authors' knowledge, the effects of heat treatment temperature and the balls–to–powder ratio (BPR) on the wet milling performance, granulometry and morphology of the powders have still to be better documented. The aim of this work

is to perform a systematic investigation into the effects of these two experimental variables on particle size distributions of the powders, crystalline phase assemblage, pore volume, and morphology of sol-gel derived bioactive glass particles.

2. Materials and methods

2.1. Wet milling procedures

The raw material used in the wet milling experiments was a high-silica-content, four–component (SiO_2–CaO–Na_2O–P_2O_5) bioglass system synthesised by employing a rapid sol-gel method developed by the authors (30). This glass was prepared with a stoichiometry of 75Si–16Ca–5Na–4P (in mol%), as described elsewhere (31). The as-dried glasses were calcined in air for a fixed soaking time of 2 h at four different heat treatment temperatures (HTT) (550 ºC, 675 ºC, 800 ºC, and 925 º C). The calcination was done in three stages: 1st stage, from room temperature (RT) to 200 ºC, at the heating rate of 1 ºC min^{-1}; 2nd stage, from 200 ºC to 400 ºC, at the heating rate 2 ºC min^{-1}; and the 3rd stage from 400 ºC to the final HTT values (550 ºC, 675 ºC, 800 ºC, 925 ºC) at the heating rate of 5 ºC min^{-1}. Natural cooling to RT followed the soaking time period of 2 h at the HTT values to obtain the final glass granules. These glass granules were dry milled for 10 minutes and passed through a 200 µm mesh sieve, and then used as starting powders for all milling experiments. Wet milling in ethanol (EtOH) was carried out in a S-series-Fast mill machine, type S2-1000 (Ceramic instruments Sassuolo-Italy) under a rotational speed of 390 rpm, using a sintered alumina jar of 300 cc capacity (Ceramic instruments Sassuolo-Italy) and spherical yttria-stabilized zirconia milling balls with diameters of 10 mm (Tosoh, Tokyo, Japan). The milling experiments were conducted for different periods of time, and using different ball-to-powder mass ratios (BPR), and a constant ethanol (EtOH) mass

to powder ratio (EPR), as shown in **Table (1)**. After milling, the balls were removed using a tea strainer and the slurry was kept overnight in an oven at 60 ºC for drying. These dried, milled powders were then passed through a 63 µm mesh sieve to remove any remaining large agglomerates, and their features were assessed by the characterisation techniques described below.

2.2. Characterisation techniques

Particle size (PS) and particle size distributions (PSD) were measured using a laser diffraction particle size analyser (Coulter LS particle size analyser; Beckman Coulter, CA). All measurements were done in triplicate runs.

The specific surface areas (SSA) and the sorption isotherms of the powders were calculated using the Brunauer-Emmett-Teller (BET method, Micrometric Gemini M-2380) using N_2 as adsorbate. Standard pre-treatment conditions were 105 ºC under vacuum for 12 h.

The amorphous and crystalline phases of the samples were identified by X-ray diffraction (XRD, PANalytical XPERT-PRO Diffractometer system) using Cu-Kα radiation (Kα =1.54059 Å), within the 2θ range varying from 6−70º in steps of 0.026 s^{-1}. The diffraction patterns were compared with JCPDS standards.

The microstructure and morphology of the thermally stabilised glasses were observed by scanning electron microscope (SEM, S-4100, Hitachi, Japan) using carbon coated samples.

For density measurements, pellets with 13 mm diameter and ~2 mm thicknesses were prepared in a stainless steel die by uniaxial pressing (60 MPa) from the sixteen milled powders. The pellets were heat-treated in air in an electric furnace at the HTT investigated in this work. The heat treatment schedule included three stages: 1st stage

from RT to 200 ºC at the heating rate of 1 ºC min^{-1}; 2nd stage from 200 ºC to 400 ºC at the heating rate 2 ºC min^{-1}; and the 3rd stage from 400 ºC to each HTT investigated at the heating rate of 5 ºC min^{-1}. Natural cooling to RT followed the soaking time period of 2 h at 800 ºC. Density determination was performed using the buoyancy (Archimedes') method by immersing the samples in distilled water, in accordance with European Standard EN 993-1. The bulk density of the glass pellets was calculated via following relation:

$$\rho_b = \frac{m_1}{m_3 - m_2} \cdot \rho_w$$

Where: ρ_b is the bulk density in (g cm^{-3});

ρ_w is the density of the water, assumed to be 1 g cm^{-3};

m_1 is the mass of the dry sintered pellet measured in air;

m_2 is the mass of the sintered pellet suspended in water;

m_3 is the mass of the water saturated pellet measured in air.

3. Results and Discussion

3.1. X-ray diffraction (XRD)

Fig. 1 shows the sixteen XRD patterns of glass powders heat treated at different temperatures and wet ball milled under different values of BPR (5, 10, 15, and 20). The samples heat treated at 550 ºC (**Fig. 1–a**) and at 675 ºC (**Fig. 1–b**) are essentially amorphous, especially when the lower BPR was used (BPR = 5). With the gradual increasing of BPR, small reflections corresponding to yttrium zirconium oxide (PDF card # 04-016-2117) started appearing with increased intensity. The only possible source of yttrium zirconium oxide is the milling media. Therefore, these results indicate that the more frequent collisions among the balls with increasing BPR

enhance the production of wear debris, and hence contamination. The change of the HTT from 550 ºC to 675 ºC did not induce noticeable variations in the patterns. Incrementing the HTT to 800 ºC promoted the formation of some poorly crystalline phases of hydroxyapatite (HAp, PDF card # 01-080-3956) and cristobalite (SiO_2, PDF card # 04-008-7640) in the sample milled with BPR = 5, as deduced from the broad and relatively low intensity of the main XRD peaks of these two phases displayed in **Fig. 1–c**. With the gradual increase of BPR, the intensities of the peaks corresponding to these two phases tended to steadily fade, while new peaks attributed to yttrium zirconium oxide (PDF card # 04-016-2117) appear with increasing intensities. Further increasing the HTT to 925 ºC resulted in glass ceramics with two new, well-developed silicon oxide (SiO_2) phases - Octadecasil (PDF card # 00-048-0476), and Unnamed zeolite (PDF card # 01-073-3446), as shown in the XRD patterns displayed in **Fig. 1–d**. The crystalline phases identified at 800 ºC had apparently disappeared, although it is likely that the intensities of their corresponding peaks are too low in comparison to the high intensity peaks of the new silica peaks formed at 925 ºC. Concerning the effects of varying the BPR, it is worth mentioning the steady reduction of the degree of crystallinity of the samples with increasing values of this experimental variable. It can be concluded that the higher energetics of the milling process, in the presence of higher amounts of balls, tend to gradually destroy the crystalline phases formed, with the resulting powders becoming progressively more amorphous. The same trend was observed for the phases initially formed at 800 ºC.

3.2. Influence of BPR and HTT on the relevant features of powders

3.2.1. Particle size (PS) & particle size distribution (PSD)

Fig. 2(a–d) shows the influence of BPR on PS and PSD for the four HTTs tested. Almost the same evolving trend can be observed irrespective of the HTT. The increase in BPR tends to decrease the average PS, and to reduce the width (span) of the PSD, with curves gradually shifting towards the left (smaller particle sizes) and becoming sharper as BPR increases. In other words, increasing both BPR and HTT led to a narrowing of the PSD, and an increase in the volume % of fine particles. However, comparing the effects of both of these variables on the milling efficiency, it can be clearly concluded that BPR plays the major role, and exerts a greater effect in both PS and PSD, than HTT.

Fig. 3(a–d) also shows the influence of BPR and HTT on PS and PSD, but with the series arranged according the HTT tested, to observe more easily the effects of variation in BPR. It can be seen that the lower HTT result in broader PSDs. The PSD curves become gradually narrower, and almost superimposed, with increasing HTT. In other words, the effects of HTT on the PS and PSD are minimised as BPR increases towards 15 and 20. This representation of milling data complements the information provided in **Fig. 2**.

3.2.2. Mean particle size

Fig. 4 displays two complementary representations of the evolution of mean particle size for all powders as functions of the HTT (**Fig. 4–a**) and BPR (**Fig. 4–b**). From these plots it can be seen that increasing the HTT up to 800 ºC is accompanied by a small decrease in the mean particle size for all BPR values, suggesting an enhanced milling efficiency. This can be understood considering that the porous structure of the particles/agglomerates makes them less fragile. Therefore, the collisions with the balls are cushioned, and milling is less effective. Further increasing the HTT from 800 ºC

to 925 ºC reverses this tendency, and the material becomes less prone to particle size reduction. This is consistent with the gradual elimination of porosity, and the formation of hard agglomerates that become more difficult to destroy upon milling.

On the other hand, increasing the BPR from 5 to 20 at constant temperature always resulted in a tremendous decrease of mean particle size, as can be seen clearly from **Fig. 4–b**. Significant reductions in mean particle size occurred at the lower HTT (550 ºC and 675 ºC) and for BPR values between 5, and 10. At higher values of HTT (800 ºC and 925 ºC) and of BPR (15 and 20), smaller reductions in the mean diameter can be observed. The overall results show that BPR plays the measure role in final particle size. These results are in a good agreement with the particle size distribution curves discussed above.

3.2.3. Specific surface area (BET–SSA) and sorption isotherms

Fig. 5 displays two complementary representations of the evolution of the specific surface area of the powders versus HTT (**Fig. 5–a**), and as a function of BPR at fixed values of HTT (**Fig. 5–b**). It can be seen that increasing both experimental variables causes drastic reductions in the SSA, especially for the samples heat treated at the lower temperatures (550 ºC and 675 ºC). The noticeable reductions in SSA caused by increasing HTT can easily be understood, as micropores in the structures obtained at lower temperatures will tend to gradually disappear due to the sintering process (32). All the curves displayed in **Fig. 5 (a)** tend to converge for temperatures ≥800 ºC. In this elevated temperature range (≥800 ºC), the SSA is practically unaffected by the milling conditions (little change with increasing BPR), while at lower HTT (550 ºC and 675 ºC), the BPR also plays a role in determining the noticeable reduction in

SSA, which decreases almost linearly with increasing BPR, and with decreasing kinetics with increasing HTT. At first glance these results seem inconsistent, as higher values of SSA would be expected when considering the decreasing PS trends inferred from the results displayed in (**Figs. 2-4**). These results are in a good agreement with the results obtained by Chauruka et al. (33). However, sol-gel derived powders usually exhibit complex porous structures, including open pores communicating with the external surface at two ends (through–pores), dead-end pores with narrow pore necks (bottleneck pores), and closed pores (34).

Closed pores are not associated with adsorption and permeability of molecules, while nitrogen condensation is likely to occur in open pores and be accompanied by hysteresis, depending on the pore size and shape. The nitrogen sorption isotherms of the bioactive sol gel glass powders submitted to different HTT and BPR upon wet milling are displayed in **Fig. 6**. All of them are Type IV(a) isotherms, according to the IUPAC classification (35), and capillary condensation is accompanied by hysteresis. For nitrogen adsorption at 77 K, hysteresis starts to occur for pores wider than ~4 nm, and when bottleneck type pores are present (34,35).

Fig. 6–a and **Fig. 6–b** compare the nitrogen sorption isotherms of the bioactive sol gel glass samples calcined at all HTT and wet ball milled under the two lower BPR values of 5 and 10, while **Fig. 6–c** and **Fig. 6–d** provide similar comparisons for the samples heat treated at 550 ºC and 800 ºC, and milled under all BPR values tested. The highest quantity of adsorbed nitrogen (pore volume) is observed for the sample heat treated at 550 ºC and ball milled with the lowest BPR. At constant BPR, the amount of adsorbed nitrogen strongly decreased as the HTT increased. Drastic decreases are observed with increasing HTT (**Fig. 6–a–b**), and pores have been

almost eliminated in samples submitted to HTT ≥ 800 ºC due to the sintering process (32).

While at constant HT,T and under more severe milling conditions (**Fig. 6–c–d**), the increase in BPR tends to decrease the amount of adsorbed nitrogen. This means that a larger volume fraction of pores has collapsed, and that the new exposed surfaces, available for nitrogen sorption, do not compensate for the loss in gas sorption storage of the resulting porous structure. Similar behaviour was observed by Amadine et al. (36). This explains the apparent inconsistencies referred to above when considering the expected relationship between PS (**Figs. 2-4**) and SSA (**Fig. 5**). The results also show the strong dependence of nitrogen adsorption on the HTT.

The adsorption and desorption branches of nitrogen sorption isotherms are not as steep as in the Type IV models typically described in literature (32), revealing more complex pore structures, with important network effects and a larger size distribution of pore diameters and neck widths.

3.2.4. Pore size and density measurements

Pore sizes data extracted from sorption isotherms are illustrated in **Fig. 7**. **Fig. 7–a** shows a general increase in mean pore size with increasing HTT up to 800 ºC, followed by a decrease beyond this temperature. These changes are attributed to the sintering effect, in which the smaller pores are the first to be readily eliminated, justifying why the mean pore diameter increases with HTT, as only the coarser ones remain. It seems that micro porosity is practically eliminated up to 800 ºC. Beyond this temperature, at HTT = 925 ºC, these larger pores then begin to be reduced and eliminated, with a much greater degree of pore loss with larger BPRs, resulting in the

decrease of pore size seen at this temperature. It can also be seen in **Fig. 7–a**, and in **Figs. 7–b** that pore size generally decreases with increasing BPR. This is consistent with the gradual collapse of the porous structure under the more severe milling conditions, as discussed above. Similar types of pore size information could also be extracted from data gathered along the desorption branch of isotherms, as shown in **Fig. 7–c**, and in **Fig. 7–d**.

The effects of HTT and BPR on the density of sintered pellets is depicted in **Fig. 8**. A general increase in density with increasing HTT is observed up to 800 ºC, followed by a reduction in density when increasing the temperature to 925 ºC. The changes in density as a function of BPR are less noticeable, with the sample derived from the powder wet ball milled at the lowest BPR (5) having the lowest density. Increasing the BPR to 10 resulted in a general enhancement of density, probably due to a more efficient destruction of particle agglomerates, in good agreement with particle size data plotted in **Figs. 2-4**. Further increasing the BPR to 15 and 20 resulted in lower values of density in comparison to those observed for BPR = 10. This decreasing trend of density maybe due to two different causes: (i) excessive production of fine particles (**Fig. 4)**, with the particle packing ability in the green state during pressing becoming worse; (ii) possible deleterious effects on sintering coming from the contamination of the wear debris of milling media, as detected by XRD (**Fig. 1)**.

3.2.5. Morphological features of the glass powders

The morphological features of the glass powders heat treated at two selected temperatures (550 ºC, 800 ºC) and wet ball milled under the extreme values of BPR (5, 20) are presented in the micrographs of **Fig. 9–a–h**. With HTT = 550 ºC, the powders consist of clusters of primary nanoscale particles that gather together during

the condensation step of the sol-gel process forming, porous microstructures, which are susceptible to being affected by the changes in the experimental variables investigated. The sub-micron particles seen in Fig. **9-a-b** are actually clusters of nanocrystals, as can be better observed in **Fig. 9-c-d**. The size of these submicron clusters diminishes from ~150-200 (**Fig. 9–c**) to ~50-100 nm (**Fig. 9–d**) as BPR increases from 5 to 20. When observed at higher magnification, these clusters at 550 ºC exhibit cauliflower–like shapes, and are built from primary nanoparticles having sizes in the range of ~10–20 nm, as depicted in **Fig. 9–c–d**. However, on a larger scale, these submicron clusters are in turn agglomerated into micron–scale agglomerations of particles (**Fig. 9-a-b**), with diameters of several microns, which leads to the particle size values measured in **Figs. 3 & 4**. These agglomerated particles also decrease in size with increasing BPR, resulting in a reduction in mean particle size.

With the HTT increasing to 800 ºC, there was little change in the dimensions of the agglomerations, with those in the BPR = 5 sample (**Fig. 9-e**) still having considerably larger sizes than those observed for BPR = 20 (**Fig. 9-f**). However, the submicron clusters had almost disappeared with BPR = 5, with only a few sub-micron clusters remaining (**Fig. 9-g**), while the submicron clusters had grown in size considerably to over 200 nm even with BPR = 20 (**Fig. 9-h**). The individual nanocrystals which made up the clusters, although still present, could also be seen to have increased in size, with HTT = 800 ºC. Although HTT clearly had an effect on the size of the individual nanocrystals and submicron clusters, the BPR exerts a much greater effect on the dimensions of the resulting agglomerations, and hence on the overall particle size, as also seen in **Figs. 3 & 4**.

Conclusions

A quaternary (Si–Na–Ca–P) bioactive sol–gel glass was heat treated at different temperatures, and wet ball-milled on a fast milling machine under constant conditions of mass of ethanol–to-powder ratio (EPR = 2) and milling time (2 h), but with four variations of ball–to-powder ratio (BPR). These were also then heated at four different heat treatment temperatures (HTT). The characterisation analyses of the resulting sixteen powder samples enabled us to draw the following conclusions:

1. Crystalline phase assemblages: The sol–gel glass remained essentially amorphous upon heating at the lower HTT (550 ºC and 675 ºC). Poorly crystalline phases (HAp and cristobalite) formed at 800 ºC, and could be easily identified in the sample milled under BPR = 5. The intensities of the XRD peaks of these two phases tended to steadily fade with increasing BPR, while yttrium zirconium oxide phase gradually appeared, resulting from wear debris of the milling media. The increase of HTT to 925 ºC led to the formation of two well crystallised silicon oxide phases, and to the apparent disappearance of the poorly crystalline phases formed at 800 ºC, which were possibly masked by the much larger XRD intensity peaks of the new silica phases.
2. Particle size & size distributions: the BPR played the major role in determining these features, especially at the lower HTTs. Particle size decreased and particle size distributions showed a clear narrowing trend with increasing BPR, irrespective of HTT.
3. BET specific surface area, sorption isotherms and pore sizes: The SSA tended to consistently decrease with increasing the HTT. Unexpectedly from the decreasing trend observed for PS, SSA clearly decreased with increasing the BPR, especially for samples heat treated at lower HTT (550 ºC and 675 ºC).

This evolution is due to the gradual collapse of the porous structure that decreases its nitrogen storage capacity. For samples heat treated at 800 ºC and 925 ºC, the effect of BPR on SSA was negligible. The gradual initial elimination of the finer pores due to advancements in the sintering process resulted in less porous structures, but consisting of larger mean pore sizes.

4. Sintered density increased with increasing HTT up to 800 ºC, followed by decreasing trends when sintering temperature was further increased to 925 ºC. Density was also enhanced upon increasing BPR from 5 to 10, reaching the highest values. Further increasing the BPR to 15 and 20 enriched the powders as finer particles, but wear debris from milling media accounted for a worsening of their sintering ability.

Acknowledgments

R.C. Pullar wishes to thank the FCT Grant IF/00681/2015 for supporting this work. B. A. E. Ben-Arfa thanks FCT grant BIONANOSCULP PTDC/EPH-PAT/6281/2014 for supporting him during this work. This work was developed in the scope of the project CICECO−Aveiro Institute of Materials (Ref. FCT UID /CTM /50011/2013), financed by national funds through the FCT/MEC and when applicable co-financed by FEDER under the PT2020 Partnership Agreement.

References

1. Ghosh S, Das M, Chakrabarti S, Ghatak S. Development of ceramic tiles from common clay and blast furnace slag. Ceram Int. 2002;28(4):393–400.

2. Oberacker R. Powder Compaction by Dry Pressing. In: Chen RR and I-W, editor. Ceramics Science and Technology. first edit. 2013. p. 1–37.

3. Richerson DW. Modern Ceramic Engineering: Properties, Processing, and Use in Design. second edi. New Jersey: Marcel Dekker, inc.; 1992.

4. Lam SSY, Petri KL, Smith AE. Prediction and optimization of a ceramic casting process using a hierarchical hybrid system of neural networks and fuzzy logic. IIE Trans Des Manuf. 1999;1381:83–4.

5. Ferreira JMF, Diz HMM. Influence of pH on the pressure slip casting of silicon carbide bodies. J Eur Ceram Soc. 1997;17(2–3):259–66.

6. Mei S, Yang J, Ferreira JMF. The fabrication and characterisation of low-k cordierite-based glass-ceramics by aqueous tape casting. J Eur Ceram Soc. 2004;24(2):295–300.

7. Ferreira JMF. Role of the clogging effect in the slip casting process. J Eur Ceram Soc. 1998;18(9):1161–9.

8. Lyckfeldt, O.; Ferreira JMF. Processing of porous ceramics by 'Starch Consolidation'. J Eur Ceram Soc. 1998;18:131–40.

9. Omatete OO, Janney M a., Nunn SD. Gelcasting: From laboratory development toward industrial production. J Eur Ceram Soc. 1997;17(2–3):407–13.

10. Gauckler LJ, Graule T, Baader F. Ceramic forming using enzyme catalyzed reactions. Mater Chem Phys. 1999;61(1):78–102.

11. Kosmac T, Novak S, Sajko M. Hydrolysis-assisted solidification (HAS): A new setting concept for ceramic net-shaping. J Eur Ceram Soc. 1997;17(2–3):427–32.

12. Xu X, Ferreira JMF. Temperature-induced gelation of concentrated sialon suspensions. J Am Ceram Soc. 2005;88(3):593–8.

13. Olhero SM, Kaushal A, Antunes P, Ferreira JMF. Microfabrication of high aspect ratio BST pillar arrays by epoxy gel casting from aqueous suspensions with added water soluble epoxy resin. Mater Res Bull. Elsevier Ltd; 2015;60(1):830–7.

14. Torralba JM, Campos M. Toward high performance in Powder Metallurgy. Rev Metal. 2014;50(2):1–14.

15. Chia HN, Wu BM. Recent advances in 3D printing of biomaterials. J Biol Eng. 2015;9(1):1–14.

16. Feilden E, Blanca EGT, Giuliani F, Saiz E, Vandeperre L. Robocasting of structural ceramic parts with hydrogel inks. J Eur Ceram Soc. 2016;36(10):2525–33.

17. Field JE, Farhat M, Walley SM. Comminution limit (CL) of particles and possible implications for pumped storage reservoirs. J Mater Sci. 2014;49(10):3780–4.

18. Loh ZH, Samanta AK, Sia Heng PW. Overview of milling techniques for improving the solubility of poorly water-soluble drugs. Asian J Pharm Sci. Elsevier Ltd; 2014;10(4):255–74.

19. Oliveira MILL, Chen K, Ferreira JMF. Influence of the deagglomeration procedure on aqueous dispersion , slip casting and sintering of Si 3 N 4 -based ceramics. 2002;22:1601–7.

20. Bentzon MD, Andersen LO, Goul J, Bodin P, Vase P. Influence of the Powder Calcination Temperature on the Microstructure in Bi (Pb) -2223 Tapes. IEEE Trans Appl Supercond. 1997;7(2):1411–4.

21. Ma B, Lu T, Wei N, Lu Z, Li F, Chen X, et al. Effect of powder calcination temperature and ceramic post-treatment on the optical properties of Nd:YAG ceramics. Int J Appl Ceram Technol. 2015;12(6):1230–8.

22. Chen Y, Dionysiou DD. Effect of calcination temperature on the photocatalytic activity and adhesion of TiO2 films prepared by the P-25 powder-modified sol-gel method. J Mol Catal A Chem. 2006;244(1–2):73–82.

23. Cai J, Xin W, Liu G, Lin D, Zhu D. Effect of calcination temperature on structural properties and photocatalytic activity of Mn-C-codoped TiO2. Mater Res. 2016;19(2):401–7.

24. Melville AJ, Rodríguez-Lorenzo LM, Forsythe JS. Effects of calcination temperature on the drug delivery behaviour of Ibuprofen from hydroxyapatite powders. J Mater Sci Mater Med. 2008;19(3):1187–95.

25. Sun S, Xu Q. Effect of calcination temperature on phase transformation and microstructure of Al2O3/GdAlO3 compound powder prepared by co-precipitation method. Key Eng Mater. 2012;512–515:535–8.

26. TEH YC, TAN CY, RAMESH S, PURBOLAKSONO J, TAN YM, CHANDRAN H, et al. Effect of calcination on sintering of hydroxyapatite. Biomaterials. 1996;17(21):2059–64.

27. Zakeri M, Ramezani M, Nazari A. Effect of ball to powder weight ratio on the mechanochemical synthesis of MoSi2-TiC nanocomposite powder. Mater Res. 2012;15(6):891–7.

28. Salili SM, Ataie A, Sadighi Z. Effect of ball size and ball to powder ratio variation on crystallite size and formation of nanocrystalline materials in

planetary ball mill. AIP Conference Proceedings. 2011. p. 127–30.

29. Lv YJ, Su J, Long YF, Cui XR, Lv XY, Wen YX. Effects of ball-to-powder weight ratio on the performance of LiFePO4/C prepared by wet-milling assisted carbothermal reduction. Powder Technol. 2014;253:467–73.

30. Ben-Arfa BAE, Miranda Salvado IM, Ferreira JMF, Pullar RC. A hundred times faster: Novel, rapid sol-gel synthesis of bio-glass nanopowders (Si-Na-Ca-P system, Ca:P = 1.67) without aging. Int J Appl Glas Sci. 2017;8:337–43.

31. Ben-Arfa BAE, Fernandes HR, Salvado IMM, Ferreira JMF, Pullar RC. Effects of catalysts on polymerization and microstructure of sol-gel derived bioglasses. J Am Ceram Soc. 2018;1–9.

32. Nogami M, Moriya Y. Glass formation through hydrolysis of Si(OC2H5)4 with NH4OH and HCl solution. J Non Cryst Solids. 1980;37:191–201.

33. Chauruka SR, Hassanpour A, Brydson R, Roberts KJ, Ghadiri M, Stitt H. Effect of mill type on the size reduction and phase transformation of gamma alumina. Chem Eng Sci. Elsevier; 2015;134:774–83.

34. Zdravkov BD, Čermák JJ, Šefara M, Janků J. Pore classification in the characterization of porous materials: A perspective. Cent Eur J Chem. 2007;5(2):385–95.

35. Thommes M, Kaneko K, Neimark A V., Olivier JP, Rodriguez-Reinoso F, Rouquerol J, et al. Physisorption of gases, with special reference to the evaluation of surface area and pore size distribution (IUPAC Technical Report). Pure Appl Chem. 2015;87(9–10):1051–69.

36. Amadine O, Essamlali Y, Fihri A, Larzek M, Zahouily M. Effect of calcination

temperature on the structure and catalytic performance of copper–ceria mixed oxide catalysts in phenol hydroxylation. RSC Adv. Royal Society of Chemistry; 2017;7(21):12586–97.

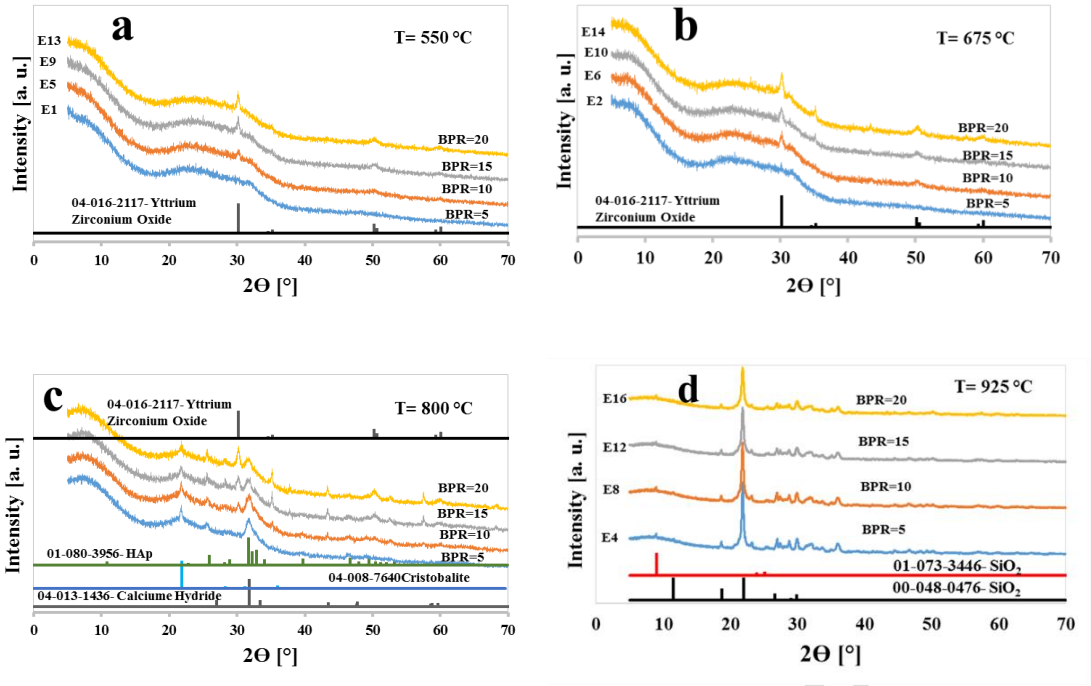

Fig. 1. *XRD patterns of the bioactive sol–gel glass powders heat treated at different temperatures [a) 550 ºC, b) 675 ºC, c) 800 ºC, d) 925 ºC] followed by wet ball milling in ethanol under four values of BPR (5, 10, 15, 20)*

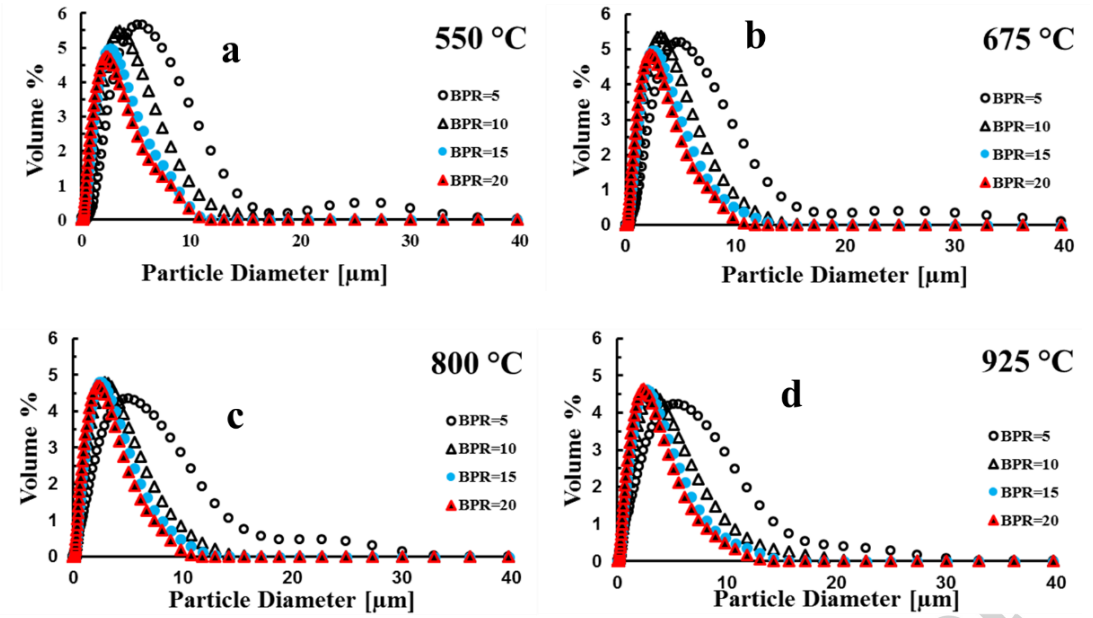

Fig. 2 *Particle size distributions of the bioactive sol-gel glass powders heat treated at different temperatures [a) 550 ºC, b) 675 ºC, c) 800 ºC, d) 925 ºC] followed by wet ball milling in ethanol under four values of BPR (5, 10, 15, 20).*

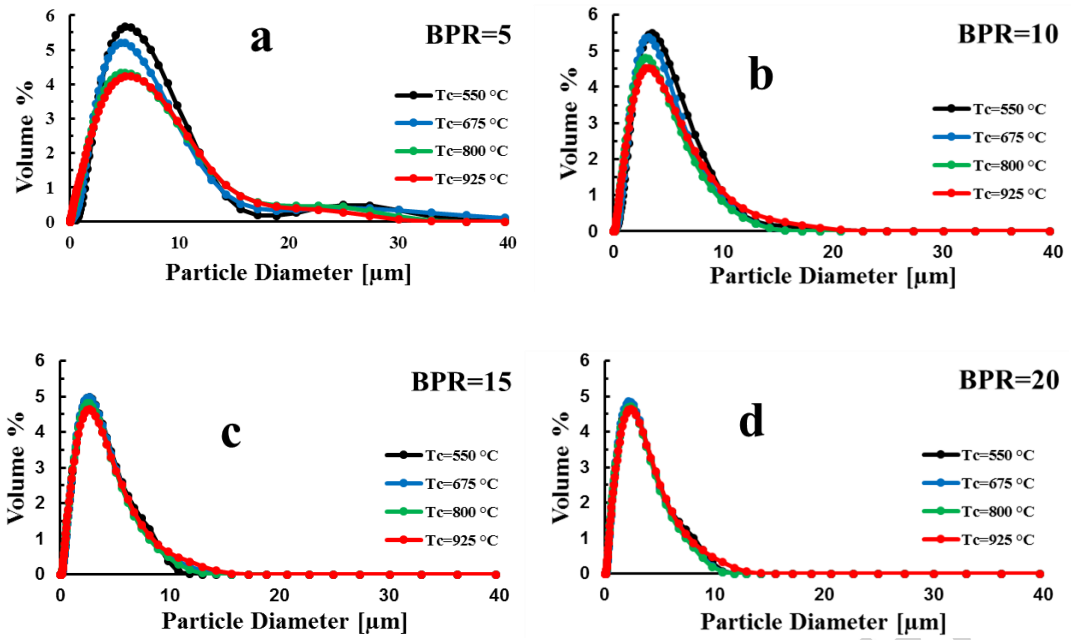

Fig. 3 *Particle size distributions of the bioactive sol-gel glass powders heat treated at different temperatures followed by wet ball milling in ethanol under given values of BPR: a) 5; b) 10; c) 15; d) 20.*

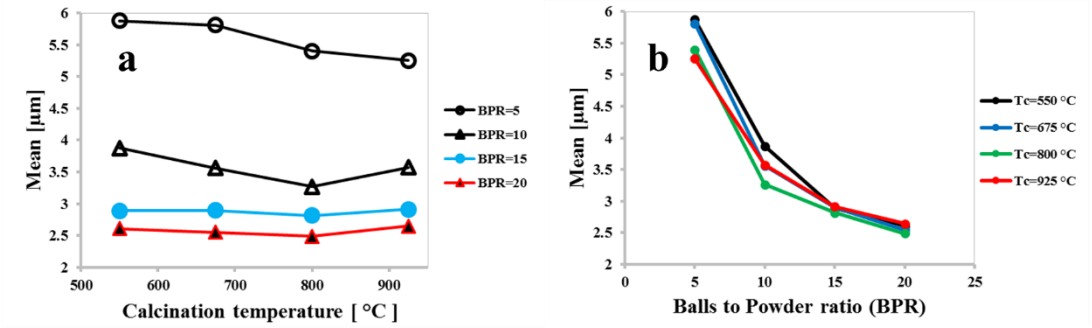

Fig. 4 *Effects of the processing parameters on the mean particle size of the bioactive sol-gel glass powders: (a) heat treatment temperature (550, 675, 800, 925 ºC); (b) BPR (5, 10, 15, and 20) used in wet ball milling in ethanol.*

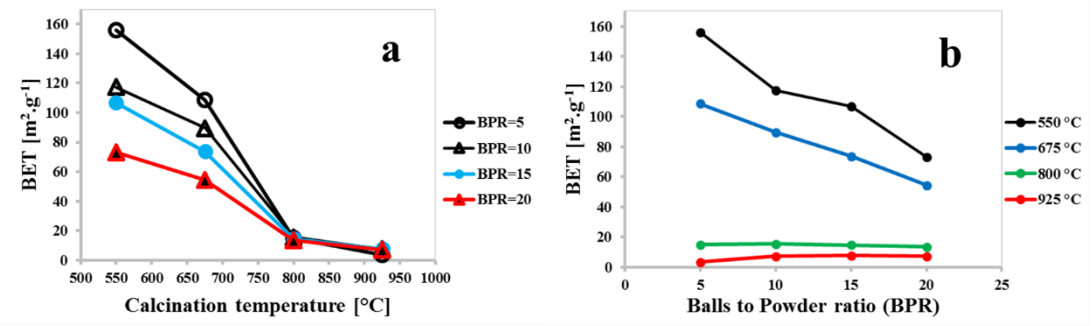

Fig. 5. *Effects of the processing parameters on the specific surface area of the bioactive sol-gel glass powders: (a) heat treatment temperature (550, 675, 800, 925 ºC); (b) BPR (5, 10, 15, and 20) used in wet ball milling in ethanol.*

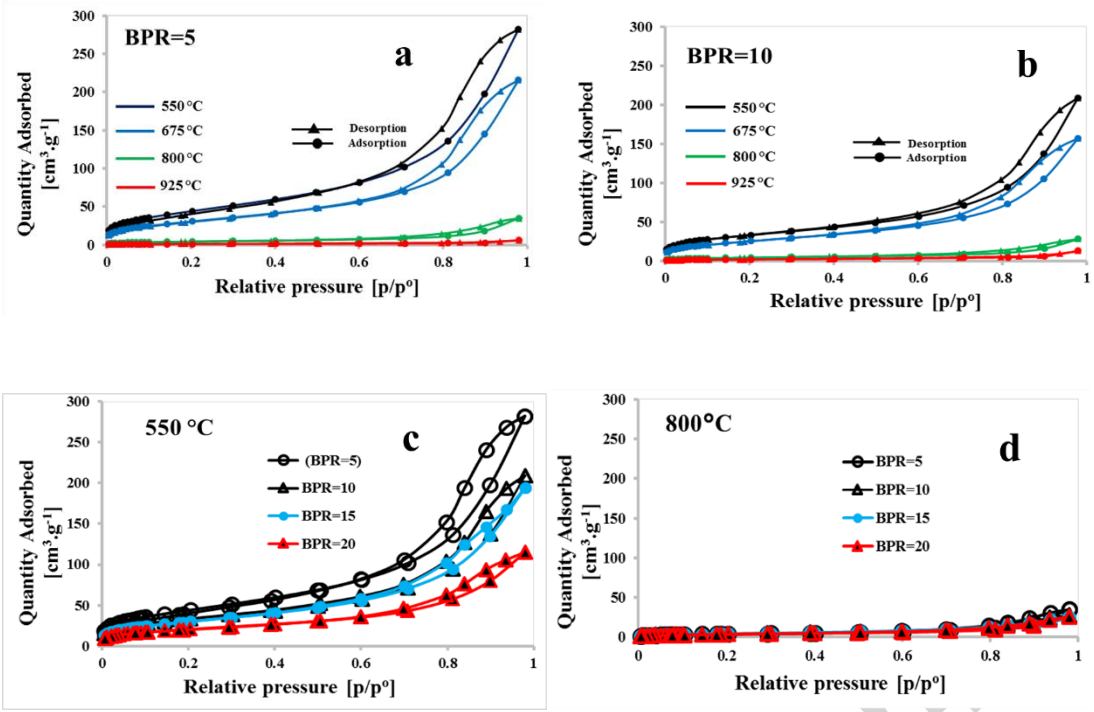

Fig. 6. *Effects of the processing parameters on the nitrogen sorption isotherms for the bioactive sol-gel glass powders: (a, b) comparison of two BPR (5, 10) used in wet ball milling in ethanol for samples heat treated at different temperatures (550, 675, 800, 925 ºC); (c, d) comparison of two heat treatment temperatures for powders wet ball milling in ethanol under different BPR values (5, 10, 15, 20).*

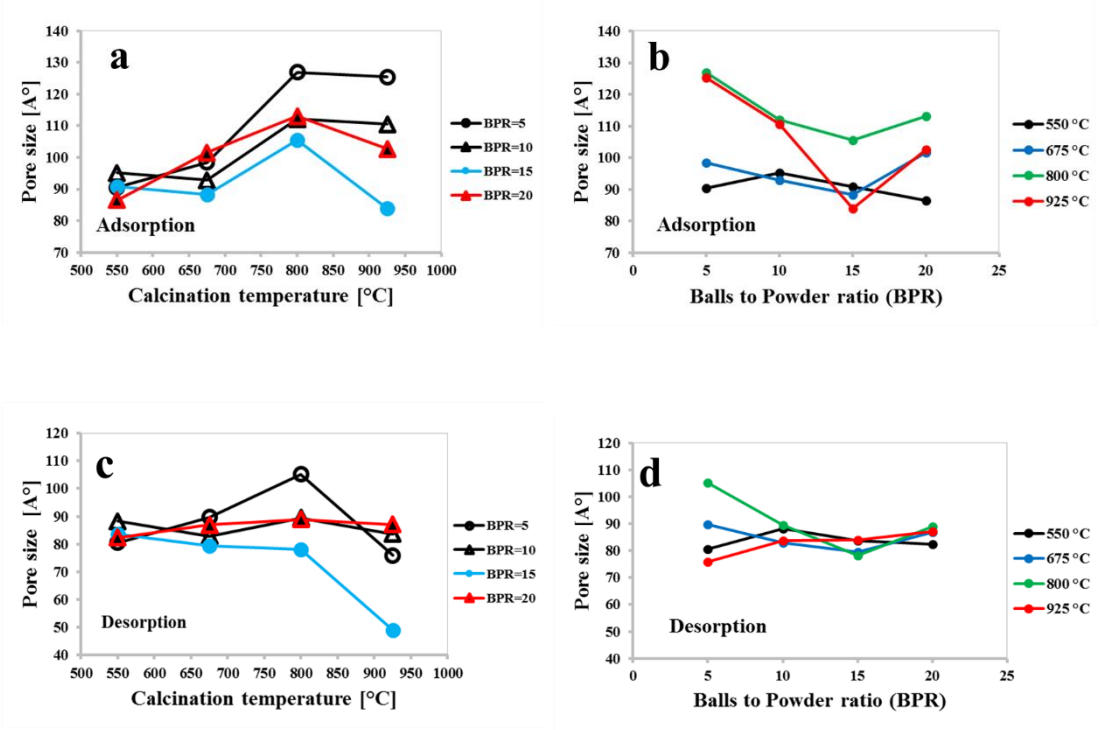

Fig. 7. *Influence of the heat treatment temperature and of the BPR used in wet ball milling in ethanol on pore size derived from sorption isotherms: (a, b) adsorption branch; (c, d) desorption branch.*

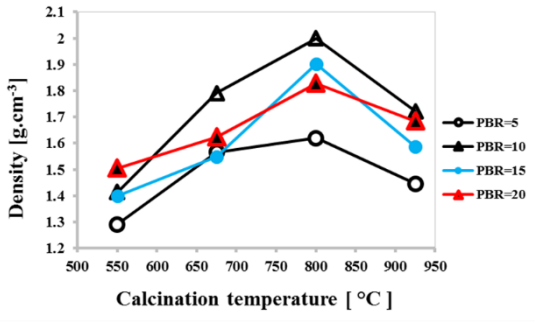

Fig. 8. *Effects of the processing parameters on the density of cylindrical pellets sintered at 800 ºC.*

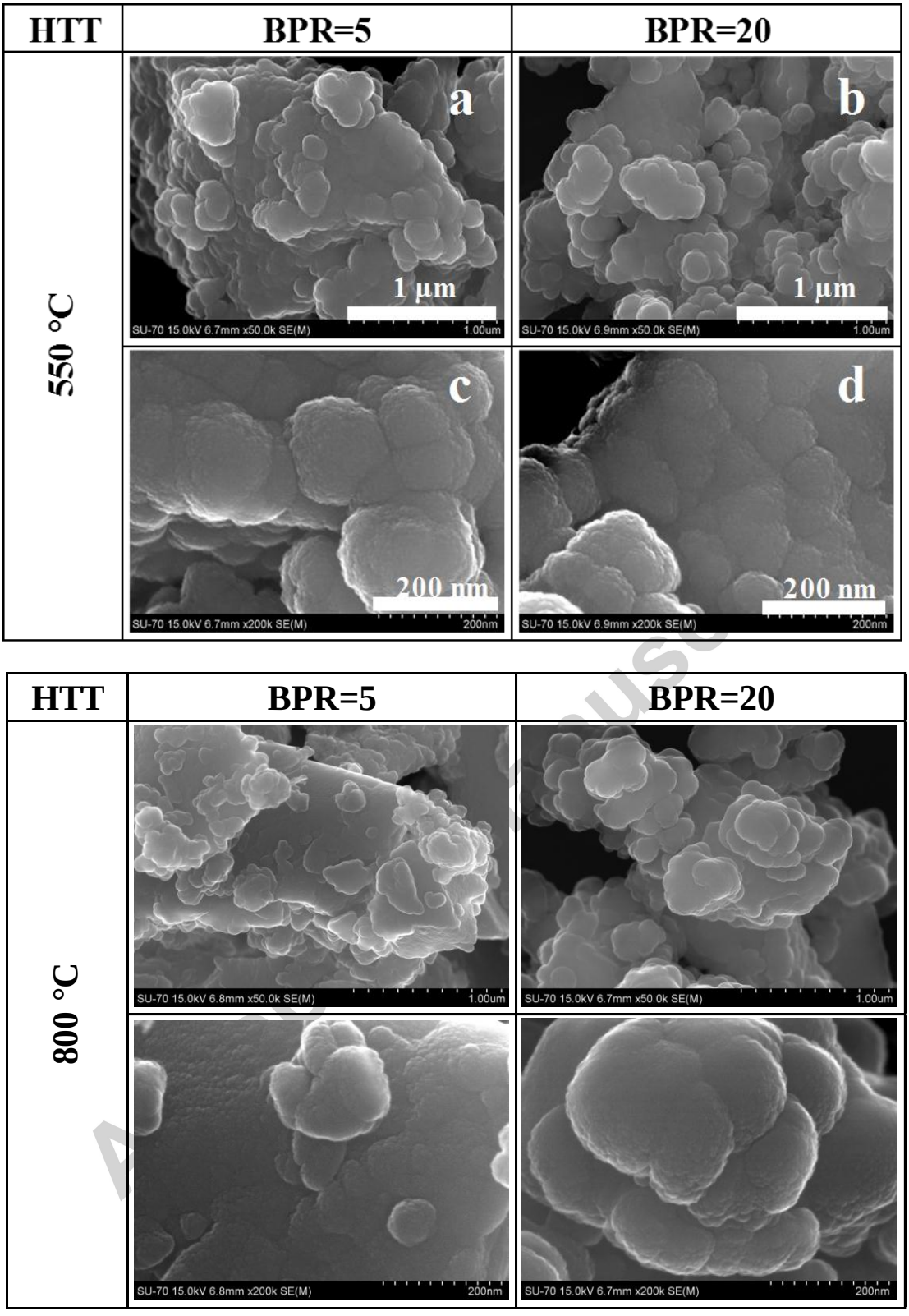

Fig. 9. *Effects of HTT (550 ºC, 800 ºC) and of BPR (5, 20) on the morphological features of the bioactive sol-gel glass powders observed under two different magnifications: 50x (a, b, e, f) and 200x (c, d, g, h).*

Table 1. The values of experimental parameters set in the 16 milling experiments. BPR = ball–to–powder ratio, EPR = ethanol-to-powder ratio, HTT = heat treatment temperature.

	Independent variables		
Trial	**BPR**	**HTT (ºC)**	**Milling time (min)**
E1	5	550	120
E2	5	675	120
E3	5	800	120
E4	5	925	120
E5	10	550	120
E6	10	675	120
E7	10	800	120
E8	10	925	120
E9	15	550	120
E10	15	675	120
E11	15	800	120
E12	15	925	120
E13	20	550	120
E14	20	675	120
E15	20	800	120
E16	20	925	120